

# Erratum: Photovoltage from ferroelectric domain walls in BiFeO<sub>3</sub>

Sabine Körbel and Stefano Sanvito

*School of Physics, AMBER and CRANN Institute, Trinity College, Dublin 2, Ireland\**

In the original article a mistake in the methodology lead to an incorrect prediction of exciton delocalization below a critical exciton density. This unrealistic delocalized exciton state yielded a sizable domain-wall photovoltage. When done correctly, the simulations yield self-trapped (localized) excitons at all considered exciton densities, without any evidence for a transition to a delocalized exciton. This realistic self-trapped exciton state yields only a negligible domain-wall photovoltage. The original conclusion that ferroelectric domain walls could be responsible for the measured photovoltage if carrier lifetime and diffusion length are higher than expected is incorrect. Correct is: The domain-wall photovoltage in BiFeO<sub>3</sub> is much too small to explain the measured photovoltage. The original analysis is meaningful for ferroelectrics without carrier self-trapping, not for BiFeO<sub>3</sub>.

Keywords: Condensed Matter & Materials Physics, Ferroelectric Domains, First-principles calculations, DFT+U, Photovoltaic Effect, Exciton, Perovskite

The mistake in the original article consists in modeling  $M$ -fold diluted exciton polarons by means of a fraction  $1/M$  of an exciton polaron ( $M \gg 1$ ) instead of using an  $M$ -times as large simulation box. This fractional-exciton approach has no predictive power for polarons. It will always predict vanishing atomic displacements and delocalized excitonic states for low exciton concentrations. This is because the atomic displacements that cause carrier self-trapping should be approximately proportional to the amount of excess charge  $|\psi|_{\text{excess}}^2$  [see Sio et al., Phys. Rev. Lett. 122, 246403 (2019), Eq. (3)], here  $|\psi|_{\text{excess}}^2/M$  with  $M \gg 1$ . When we perform the simulation correctly with an integer number of charge carriers in a larger supercell, we observe self-trapping for all supercell sizes considered (up to 320 atoms, see section “Self-trapping at low carrier concentrations” in the Supplemental Material [1]).

The original article is affected by the mistake as follows:

**Incorrect in the original:** The original statement that there was a transition between self-trapped and delocalized exciton is incorrect. Figures 3(a), Fig. 4, and Fig. 5 of the original article are wrong. In the original article, based on a fractional-exciton approach, we wrongly stated that at sufficiently low exciton densities, the excitons were delocalized. A fractional-exciton approach is only meaningful for a hypothetical ferroelectric that does not exhibit charge-carrier self-trapping. Such a ferroelectric may or may not exist. BiFeO<sub>3</sub> is not such a ferroelectric. For BiFeO<sub>3</sub> it is necessary to consider self-trapping of charge carriers. The original conclusion that ferroelectric domain walls in BiFeO<sub>3</sub> can account for photovoltages of the order of the experimentally measured  $\approx 10$  mV per domain, if carrier lifetimes and diffusion lengths are large, is incorrect.

**Correction:** Part of the original results obtained without carrier self-trapping are still meaningful. We assume that before self-trapping of an exciton is completed, the exciton is delocalized, and the fractional-exciton approach can be

used to calculate the domain-wall photovoltage as it was done in the original article. Once self-trapping of the exciton is completed, the exciton no longer contributes to the domain-wall photovoltage because it has lost its dipole moment, see Fig. 3, and the domain-wall photovoltage is approximately zero until the end of the exciton lifetime. The measurable domain-wall photovoltage is a time average. When carrier self-trapping is correctly accounted for, the domain-wall photovoltage of BiFeO<sub>3</sub> is lower than the experimentally measured one by orders of magnitude, indicating that the measured photovoltage of BiFeO<sub>3</sub> should arise from other causes than pristine ferroelectric domain walls.

**Addition:** To determine the time needed for carrier self-trapping, we performed molecular dynamics simulations of excitons at ferroelectric domain walls.

The individual sections of the original article are affected by the mistake as follows:

## INTRODUCTION

**Correct in the original:** The original Introduction is correct.

**Addition:** First we consider domain-wall electrostatics in the ground state, without photo-generated charge carriers, to determine the potential energy landscape that photocarriers experience. Next, we add electron-hole pairs, forbidding changes in the atomic positions (forbidding self-trapping of excitons), and show that in this case the domain walls separate electron and hole and can give rise to a photovoltage about as large as the one measured in experiment. This idealized case corresponds to a BiFeO<sub>3</sub>-like ferroelectric without exciton self-trapping, which may or may not exist. Finally, we consider real BiFeO<sub>3</sub> and take into account unavoidable changes in the atomic coordinates (we allow for spontaneous self-trapping of the excitons), and show that now the domain walls no longer separate electron and hole: electron-hole attraction is stronger. In the self-trapped exciton

state (small exciton polaron), both electron and hole reside on the same side of the domain wall.

## METHODS

**Correct in the original:** The original Methods section is correct.

### Domain walls without excitons

The part of the original Methods section about domain walls without excitons is correct.

### Domain walls with excitons

**Addition:** We perform two types of calculations with electron-hole pairs (excitons) at ferroelectric domain walls:

1) Atomic positions fixed. This case corresponds to a hypothetical ferroelectric material which does not exhibit self-trapping of carriers. The domain-wall photovoltages obtained for this hypothetical ferroelectric tell us how large domain-wall photovoltages in ferroelectrics can in principle become. We calculate the domain-wall photovoltage from the electronic potential and correct it for ionic screening by means of an effective dielectric constant. Here we consider different exciton concentrations by means of fractional occupations of electron and hole state. This fractional-exciton approach is valid only if atomic displacements caused by the exciton (polaronic effects) can be neglected.

2) Atomic positions optimized (we allow for carrier self-trapping). The calculations take longer, therefore smaller supercells are used. These calculations correspond to real  $\text{BiFeO}_3$ , as far as DFT+ $U$  calculations can represent a real material. These calculations tell us how large the domain-wall photovoltage can become in  $\text{BiFeO}_3$  and similar materials that exhibit carrier self-trapping. Since polaronic effects are important, here it is necessary to consider an integer number of excitons in the simulation box.

**Modification:**

#### *Atomic coordinates fixed*

Calculations were performed using supercells with 280 atoms. Exciton concentrations from 0.005 to 0.1 excitons per 280-atom supercell were considered. Only the electronic density was optimized, cell parameters and atomic positions were kept fixed to their ground-state values. Hence, self-trapping of excitons (small exciton polaron formation) was forbidden.

#### *Atomic coordinates optimized*

Calculations were performed in supercells containing 120 atoms. We consider a single exciton concentration of one exciton per 120-atom supercell. Both the atomic positions and cell parameters were optimized until the energy difference between subsequent ionic relaxation steps fell below 0.1 meV. Hence, self-trapping of excitons (small exciton polaron formation) was allowed (not enforced). The domain-wall photovoltage was not calculated explicitly because the electronic potential in the optimized geometry was too noisy to extract a potential profile. However, visual inspection of the electron and hole wavefunction (Fig. 3) indicates that the exciton's dipole moment is negligible compared to the case with fixed atomic coordinates.

**Addition:**

#### *Ab initio molecular dynamics*

To determine the time needed for exciton self-trapping, we performed first-principles molecular dynamics simulations at 0 K and at 300 K to exclude and include thermal effects. In the case of room temperature, we first equilibrated the system without excitons for 500 fs. The simulations were carried out in the  $NVT$  ensemble using an Anderson thermostat with  $\nu=0.5$  (0 K) and  $\nu=0.1$  (300 K), respectively, where  $\nu$  is the probability for velocity reassignment per atom and time step. Supercells containing 120 atoms were employed. The timestep was set to 1 fs. The supercells are too small and  $\nu$  is too large to approach the thermodynamic limit, therefore the simulated dynamics can only yield an estimate for the order of magnitude of the time needed for exciton self-trapping.

## RESULTS AND DISCUSSION

### Domain walls without excitons

**Correct in the original:** The original results for domain walls without excitons are correct. The first part of the original Results section and Figures 1 and 2, which show the ferroelectric polarization and electronic potential profile at  $71^\circ$  and  $109^\circ$  domain walls, are correct.

### Domain walls with excitons

#### *Atomic coordinates fixed*

**Incorrect in the original:** The original results for domain walls with diluted (fractional) excitons and with fixed atomic coordinates are valid for a hypothetical ferroelectric that does not exhibit carrier self-trapping. Such a material may or may not exist. For  $\text{BiFeO}_3$  it is necessary to include carrier

self-trapping. The original results for the delocalized exciton state should be valid for BiFeO<sub>3</sub> for less than a picosecond after exciton formation (see below). The original Figure 6, which shows the electronic potential without and with a delocalized exciton and the domain-wall photovoltage profile, is valid for a hypothetical ferroelectric without self-trapping, or for BiFeO<sub>3</sub> before exciton self-trapping is completed. Here in a modified Fig. 6 an additional panel 6(a) shows the densities of excess electron and hole in the delocalized exciton state.

**Addition:** If we artificially fix the atomic coordinates in the presence of an electron-hole pair, corresponding to an idealized ferroelectric without exciton self-trapping, then the exciton is delocalized and split by the domain wall, with the hole on the left and the electron on the right hand side of the wall, i.e. the exciton has a dipole moment antiparallel to the net polarization [Figs. 3(a) and 6(a)]. The potential change induced by the exciton determines the domain-wall photovoltage except for the ionic screening, which is added afterwards by means of an effective dielectric constant.

#### Atomic coordinates optimized

**Incorrect in the original:** The original results for domain walls with a fraction of an exciton and with optimized atomic coordinates are wrong. The original claim that excitons are delocalized below a critical exciton density is incorrect. The top panel of the original Figure 3 showing a delocalized spatial distribution of diluted excitons is wrong. The original Figure 4, depicting densities of diluted excitons and exciton formation energies after optimization of atomic coordinates, is wrong. The original Figure 5, depicting a phase diagram for excitons with stability regions of a delocalized and a self-trapped exciton state, is wrong. Original text sections corresponding to the original Figures 3(a), 4, and 5 are wrong.

**Correct in the original:** The original results for domain walls with an integer exciton in the supercell, depicted in the original Fig. 3(b), are correct.

**Addition:** Initially the exciton is split by the domain wall and exhibits a dipole moment [see Fig. 3(a)]. When changes in the atomic positions are allowed, the exciton becomes spontaneously self-trapped, see Fig. 3(b). After self-trapping both electron and hole reside on the same side of the domain wall and the exciton's dipole moment is lost. Carrier self-trapping destroys the domain-wall photovoltage.

#### Ab initio molecular dynamics

**Addition:** How long does self-trapping of excitons take? By means of molecular dynamics we show that the exciton self-trapping happens so fast that most of its lifetime the exciton

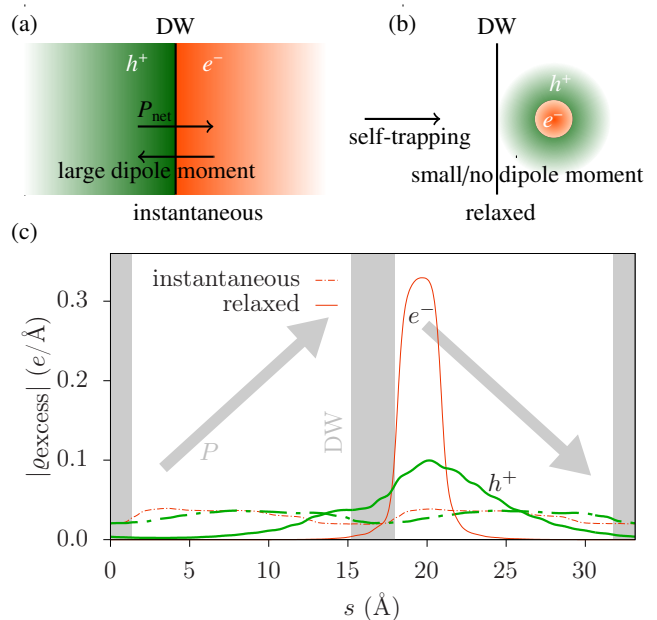


FIG. 3. **Modification:** (a) and (b) Sketch of self-trapping of an exciton at a ferroelectric domain wall (DW). (c) Smoothened densities of excess electron and hole for excitons at the 71° domain wall before (“instantaneous”) and after (“relaxed”) optimization of the atomic coordinates, i. e. exciton self-trapping. The exciton density is 1 exciton per 120-atom supercell ( $\approx 2.3 \cdot 10^{14}/\text{cm}^2$ ). Gray bars and arrows indicate ferroelectric domains.

is in the self-trapped state for carrier lifetimes  $\gg 1$  ps, see below. Figure 4 shows the total energy change with respect to the delocalized exciton state, local magnetic moments of Fe atoms, and real simulation temperature for a target temperature of 0 K as a function of time, and the charge densities of excess electron and hole at different times during the simulation. The energy gained by exciton self-trapping (small exciton polaron formation) is about 0.3 eV (the energy difference between  $t = 0$  and  $t \rightarrow \infty$ ). Carrier self-trapping is revealed by the change in magnetic moment of one Fe atom, where the excess electron localizes. This localization happens abruptly in a time interval of the order of 10 fs [see inset in Fig. 4(b)]; it is accompanied by an abrupt decrease in total energy [see inset in Fig. 4(a)]. Afterwards the system continuously lowers its energy further during several hundred femtoseconds [Fig. 4(a)]. No activation barrier for localization is visible. Note that the precise numerical value of the local magnetic moment is not meaningful, as it depends on the radius chosen for the projection on the Fe atoms; the expected value for an Fe<sup>3+</sup> ion without excess charge would be  $5 \mu_B$  (observed here:  $\approx 4 \mu_B$ ). At 300 K (Fig. 5) the exciton localizes instantaneously (one magnetic moment is much smaller than the others already in the first time step). Other than at 0 K, the exciton localizes in some distance from the domain wall, indicating that thermal fluctuations of atomic positions are more important than the trapping potential of the domain walls. The position of the self-trapped exciton changes between 0 and 9 fs, indicat-

ing that the thermal energy at room temperature is sufficient to overcome the barrier for exciton hopping. The second reduced magnetic moment belongs to an Fe atom carrying a localized hole, see Fig. 5(b) and (f). We find that the hole part of the exciton is strongly localized, other than the individual hole [2]. The time needed for carrier self-trapping (small polaron formation) could increase with decreasing exciton density. Allowing for an unphysical influence of supercell size, thermostat parameter, and exciton density on the simulated dynamics, we estimate 1 ps as an upper limit for the time needed for exciton self-trapping.

### Domain-wall photovoltage

**Incorrect in the original:** The original Figure 7 showed the domain-wall photovoltage of a hypothetical ferroelectric without exciton self-trapping, not of BiFeO<sub>3</sub>.

**Correction:** We consider two cases, one hypothetical, one real. The hypothetical case is a BiFeO<sub>3</sub>-like ferroelectric without carrier self-trapping. Its domain-wall photovoltage is calculated assuming that the excitons remain in their delocalized state and are split by the domain wall throughout their lifetime. Figure 7 depicts these hypothetical domain-wall photovoltages (empty symbols), which are identical to those in the original Fig. 7. In addition, the new Fig. 7 depicts also the domain-wall photovoltages of real BiFeO<sub>3</sub>, which are extremely small due to fast self-trapping of carriers, as we saw in the molecular dynamics section. The self-trapped exciton is no longer split over the two sides of the domain wall, it has no considerable dipole moment. The domain-wall photovoltages for this real case are calculated by assuming that the domain-wall photovoltage is that of hypothetical BiFeO<sub>3</sub> during self-trapping and zero after self-trapping (after 1 ps). This is an optimistic assumption. Figure 7 shows the time average of the calculated domain-wall photovoltage.

For a hypothetical BiFeO<sub>3</sub>-like ferroelectric without self-trapping of excitons, the calculated domain-wall photovoltage matches the experimentally measured total photovoltage per domain only in the most optimistic scenario [Fig. 7(a)], in which we assume a carrier lifetime of 75  $\mu$ s and a carrier diffusion length of 140 nm, resulting in a photocarrier density of 10<sup>16</sup>/cm<sup>3</sup> to 10<sup>18</sup>/cm<sup>3</sup>. For comparison, in Ref. [3] a carrier density of about 10<sup>12</sup>/cm<sup>3</sup> to 10<sup>13</sup>/cm<sup>3</sup>, a carrier diffusion length of 8 nm, and a lifetime of 35 ps were assumed, in Ref. 4 a lifetime of 1 ns. If we assume such conditions [Fig. 7(b), (c)], the DW-PVE is orders of magnitude too small to account for the major part of the measured photovoltage in BiFeO<sub>3</sub> even when carrier self-trapping does not occur. In real BiFeO<sub>3</sub>, where we observe spontaneous self-trapping of excitons on a sub-ps time scale, the domain-wall photovoltage is orders of magnitude lower than that of the hypothetical material and the measured total photovoltage, which shows that pristine ferroelectric domain walls cannot be responsible for the measured photovoltage of BiFeO<sub>3</sub>.

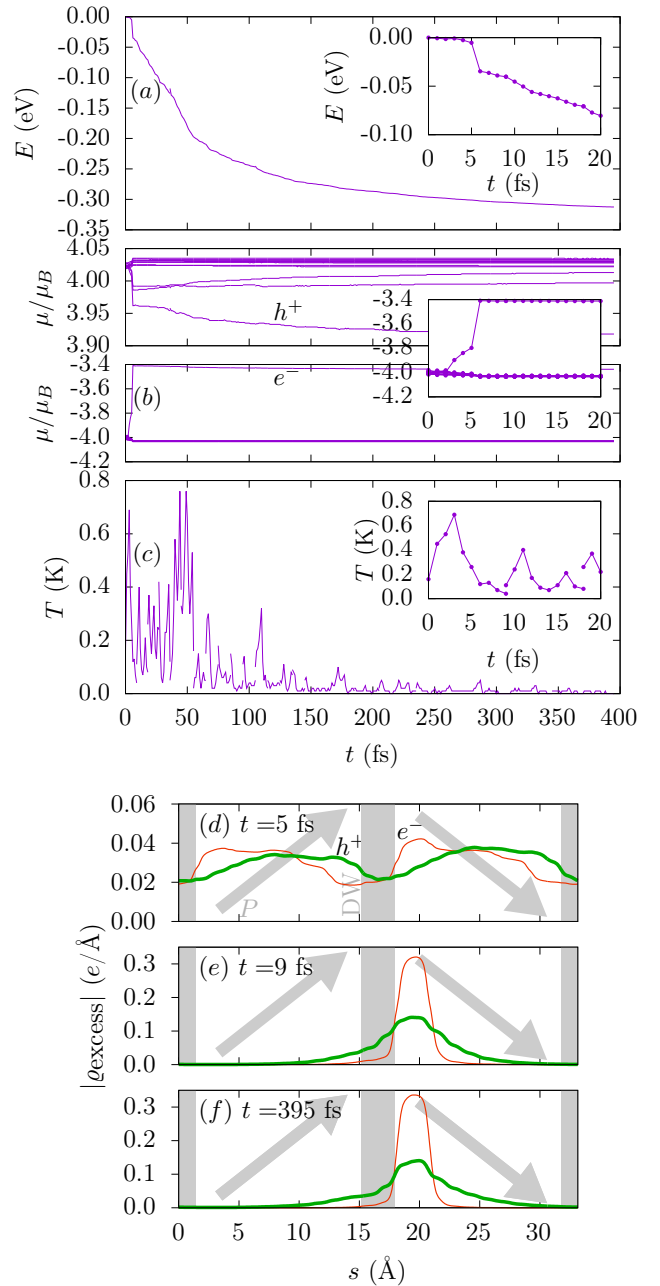


FIG. 4. **Addition:** (a) Total energy change with respect to the delocalized exciton state, (b) local magnetic moments of Fe atoms, and (c) temperature for an MD simulation with an electron-hole pair at a target temperature of 0 K. (d) to (f): planar averaged charge density of electron and hole at different times  $t$ .

### CONCLUSION

**Correct in the original:** The original conclusions that “the ferroelectric polarization profile does not allow one to determine the correct sign and magnitude of the electrostatic potential at the domain walls” and that the self-trapped exciton could be experimentally detected “as a state inside the

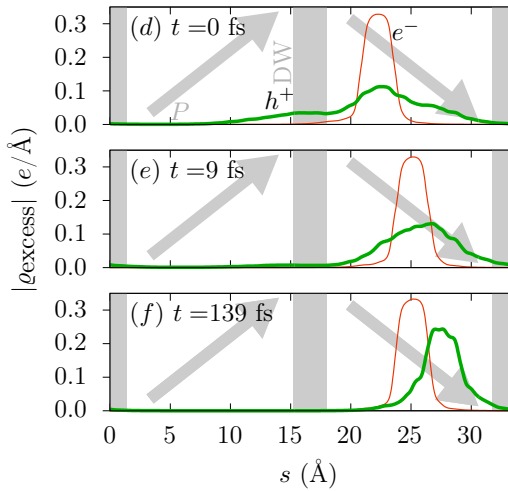
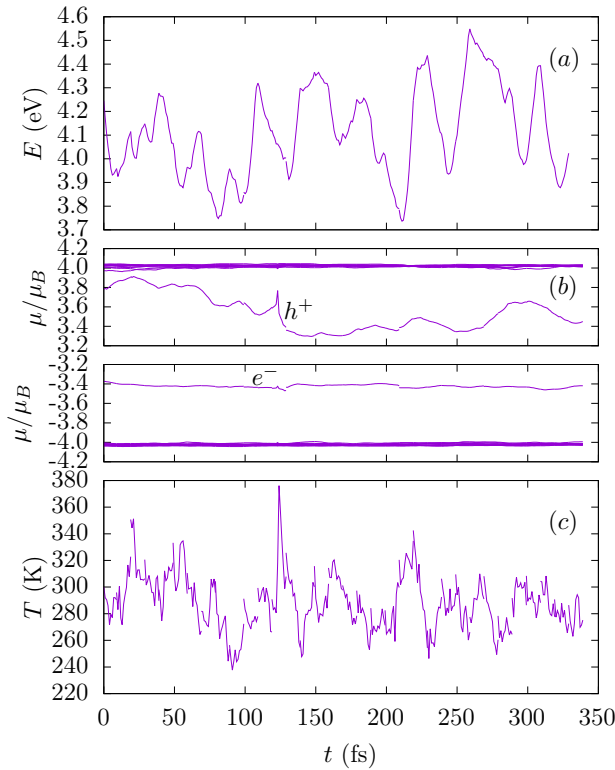


FIG. 5. **Addition:** The same as Fig. 4 for a target temperature of 300 K.

band gap in photoluminescence spectroscopy” are correct.

**Incorrect in the original:** The original conclusion that the domain-wall photovoltage in BiFeO<sub>3</sub> might be responsible for the measured photovoltage is wrong.

**Correction:** In principle, the domain-wall driven photovoltage in a ferroelectric can be as large as  $\approx 10$  mV per domain wall in ferroelectrics that do not exhibit exciton self-trapping, if the carrier lifetimes and carrier diffusion

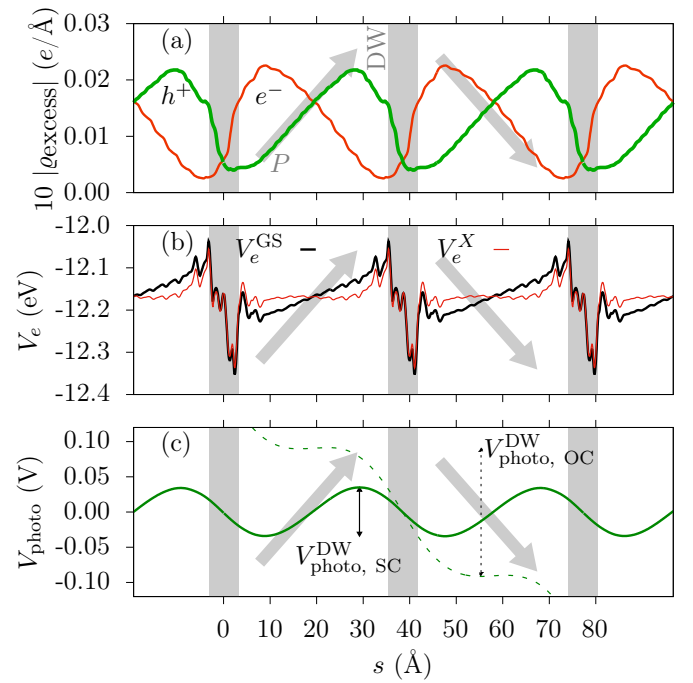


FIG. 6. **Modification:** (a) Electron and hole density at the 71° domain wall in the excited state in a 280-atom supercell with 0.1 excitons. (b) Smoothed potential energy of electrons in the ground state ( $V_e^{\text{GS}}$ ) and in the excited state ( $V_e^{\text{X}}$ ). (c) Instantaneous domain-wall photovoltage profile  $V_{\text{photo}}$  [cf. Eq. 1] for short-circuit (solid line) and open-circuit conditions (dashed line). Green arrows show the magnitude of the domain-wall photovoltage  $V_{\text{photo}}^{\text{DW}}$ .

lengths are of the order of  $\approx 100 \mu\text{s}$  and  $\approx 100 \text{ nm}$ , respectively.

We find that this is not the case for BiFeO<sub>3</sub>. We observe strong exciton self-trapping on a sub-ps timescale, which overcomes charge separation by the ferroelectric domain walls and renders the domain-wall driven photovoltage several orders of magnitude lower than the total experimentally measured photovoltage of  $\approx 10$  mV per 140-nm domain. Hence, the measured photovoltage in BiFeO<sub>3</sub> must arise from causes other than pristine ferroelectric domain walls. Note that here only domain-wall photovoltaic effects were considered, not bulk effects.

## ACKNOWLEDGEMENT

This project has received funding from the European Union’s Horizon 2020 research and innovation programme under the Marie Skłodowska-Curie Grant Agreement No. 746964 - FERROVOLT. Computation time and support provided by the Trinity Centre for High Performance Computing funded by Science Foundation Ireland is gratefully acknowledged. We also thank the Irish Centre for High-End Computing (ICHEC) for the provision of computational facilities and support. We are grateful to Subhayan Roychoudhury (Trinity College Dublin) for helpful discussions about excited-state

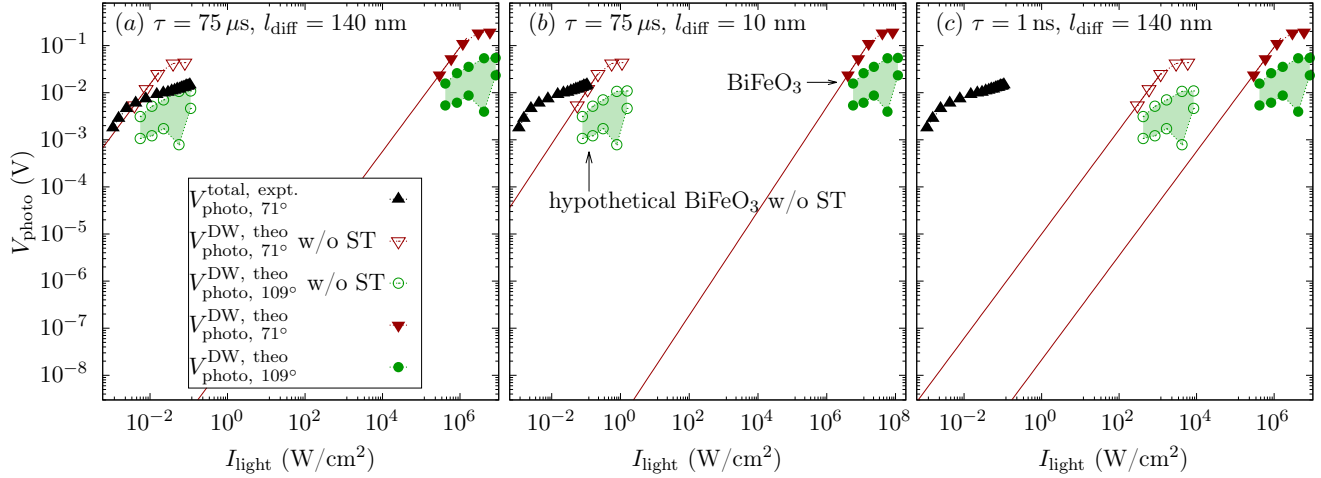


FIG. 7. **Modification:** Measured photovoltage per domain of  $\text{BiFeO}_3$  films with  $71^\circ$  domain walls from Ref. 3 and calculated domain-wall photovoltage of the  $71^\circ$  and the  $109^\circ$  domain walls as a function of the illumination intensity for different photocarrier life times  $\tau$  and diffusion lengths  $l_{\text{diff}}$ . For a hypothetical  $\text{BiFeO}_3$ -like ferroelectric without self-trapping (w/o ST, empty symbols), the domain-wall photovoltage can reach the measured total photovoltage at similar light intensities as in experiment [(a) and (b)]; when exciton self-trapping is taken into account (filled green and brown symbols), the domain-wall photovoltage is reduced by several orders of magnitude. Solid lines are an extrapolation, dotted lines are a guide to the eye.

density-functional theory. Graphics were made using gnuplot and VESTA [5].

\* skoerbel@uni-muenster.de

- [1] See Supplemental Material at <https://journals.aps.org/prb> for details .
- [2] Sabine Körbel, Jirka Hlinka, and Stefano Sanvito, “Electron trapping by neutral pristine ferroelectric domain walls in  $\text{BiFeO}_3$ ,” *Phys. Rev. B* **98**, 100104(R) (2018).

- [3] Jan Seidel, Deyi Fu, Seung-Yeul Yang, Esther Alarcón-Lladó, Junqiao Wu, Ramamoorthy Ramesh, and Joel W Ager III, “Efficient photovoltaic current generation at ferroelectric domain walls,” *Phys. Rev. Lett.* **107**, 126805 (2011).
- [4] YM Sheu, SA Trugman, Y-S Park, S Lee, HT Yi, S-W Cheong, QX Jia, AJ Taylor, and RP Prasankumar, “Ultrafast carrier dynamics and radiative recombination in multiferroic  $\text{BiFeO}_3$ ,” *Appl. Phys. Lett.* **100**, 242904 (2012).
- [5] Koichi Momma and Fujio Izumi, “VESTA3 for three-dimensional visualization of crystal, volumetric and morphology data,” *J. Appl. Crystallogr.* **44**, 1272–1276 (2011).

# Erratum: Photovoltage from ferroelectric domain walls in BiFeO<sub>3</sub>: Revised Supplemental Material

Sabine Körbel and Stefano Sanvito

*School of Physics, AMBER and CRANN Institute, Trinity College, Dublin 2, Ireland\**

Figure 4(a) in the original Supplemental Material was incorrect. So was part of the section “Excitonic densities”. In this revised Supplemental Material, errors have been corrected and a new Figure 10 and a new section “Self-trapping at low carrier concentrations” have been added.

## Calculated ground-state properties of BiFeO<sub>3</sub>

Table I contains our calculated structural parameters of BiFeO<sub>3</sub> in the *R3c* phase in comparison with experimental data. Lattice parameters deviate from experiment by about 2%, typical for LDA calculations. Ferroelectric displacements of atoms from the ideal perovskite structure deviate by up to 20%. Ferroelectric distortions of the unit cell (*c/a* ratio and rhombohedral cell angle) are severely underestimated by  $\approx 80\%$ , nevertheless the ferroelectric polarization is in good agreement with experiment, indicating that ferroelectric properties are well captured by our computational setup.

## Calculated domain-wall properties

In Table II we compare our calculated DW formation energies and widths for different supercell sizes with those available in the literature. For historical reasons, we include the 180° wall, although we do not consider it in the main article. Note that Ref. 6 found close agreement between domain-wall structures seen in electron microscopy and those calculated from first principles. This is true in particular for the domain-wall widths, which are as narrow as about one atomic layer in the case of the 109° domain wall and two atomic layers in the case of the 180° domain wall, both according to experiment and to first-principles calculations (see Fig. 1 and 2 in Ref. 6). The 71° domain wall is slightly broader and extends over about three atomic planes. We fitted the polarization and tilt profiles *P* and *A* with a tangens hyperbolicus to extract the DW width  $\xi_P$ ,

$$P_r(s) = P_r^\infty \tanh[(s - s_0)/\xi_P], \quad (1)$$

where  $P_r$  is the rotating component of the polarization,  $P_r^\infty$  is its asymptotic value far away from the domain wall, and *s* is the distance from the domain wall. In this section, different from below and the main article, polarization profiles are calculated from ionic positions and formal ionic charges (Bi<sup>3+</sup>, Fe<sup>3+</sup>, and O<sup>2-</sup>). Tests indicated that applying the more sophisticated Born effective charges changed the resulting polarization essentially only by a prefactor. The DW energies are close to those of Diéguez [7] and do not change very strongly with supercell size. Polarization and tilt profiles (Fig. 2) are also converged with respect to supercell size.

Figure 1 shows the layer-resolved ionic sublattice displacements compared to a paraelectric reference structure with-

out octahedral tilts. The displacement profiles are atomically sharp.

## Electronic potential step at the domain wall

Figure 3 depicts the magnitude of the electrostatic open-circuit potential step at the domain wall in the ground state (without excitons). These data are also listed in Table III. The potential converges to a positive number for both walls, so that it has the opposite sign compared to the polarization-based potential. We obtain the limit  $\Delta V_e^{\text{DW}}(\infty)$  of the potential step for large domain-wall distances  $d_{\text{DW}}$  by fitting with a power law:

$$\Delta V_e^{\text{DW}}(d_{\text{DW}}) = \Delta V_e^{\text{DW}}(\infty) + c \cdot d_{\text{DW}}^p, \quad (2)$$

where  $\Delta V_e^{\text{DW}}(\infty)$ , *c*, and *p* are fit parameters. The resulting exponents are  $p_{71^\circ \text{ DW}} = -2.00$  and  $p_{109^\circ \text{ DW}} = -2.07$ .

## Calculation of the polarization-based potential

The ferroelectric polarization was calculated from ionic displacements from ideal perovskite positions using direction-averaged Born effective charges  $Z^*$  of the *R3c* phase ( $Z_{\text{Bi}}^* = 4.865$ ,  $Z_{\text{Fe}}^* = 3.886$ ,  $Z_{\text{O}}^* = -2.917$ ). First a smooth curve was fitted to the polarization profile perpendicular to the domain wall [ $P_s$  in Fig. 1 (c) and Fig. 2 (c) in the main article] using the program gnuplot. We employed a symmetric fit function of the form

$$P_s(s) = P_s^{(0)} - \frac{P_s^{(1)}}{\cosh^2\left(\frac{s-s_0}{\xi}\right)}, \quad (3)$$

where  $P_s^0$ ,  $P_s^1$ ,  $s_0$ , and  $\xi$  are fit parameters. The polarization-based electronic potential was then calculated as (compare Eq. (8) in Ref. [10])

$$V_e^{\text{pb}}(s) = -\frac{1}{\epsilon_{ss}} \int_{s^-}^s (P_s(s') - P_s(s^-)) ds', \quad (4)$$

where  $s^-$  is a position in the domain interior on the left hand side of the domain wall, and  $\epsilon_{ss}$  is the calculated electronic dielectric constant for an electric field perpendicular to the domain-wall plane (see below). For  $P_s(s)$  we used the fitted curve from Eq. (3).

	Expt	ideal perovskite	this work
$a$ (Å)	5.57330(5) <sup>d</sup> ; 5.57882(5) <sup>b</sup> ; 5.5876(3) <sup>a</sup> ; 5.58132(5) <sup>c</sup> ;		5.5006 (-1.3%)
$c$ (Å)	13.84238(16) <sup>d</sup> ; 13.867(1) <sup>a</sup> ; 13.86932(16) <sup>b</sup> ; 13.87698(15) <sup>c</sup> ;		13.507 (-2.4%)
$c/a$	2.4817 <sup>a</sup> ; 2.48370 <sup>d</sup> ; 2.48607 <sup>b</sup> ; 2.48633 <sup>c</sup>	$\sqrt{6}$ $\approx 2.4495$	2.4556 (-81%)
$V$ (Å <sup>3</sup> )	372.36 <sup>d</sup> ; 373.06 <sup>f</sup> ; 373.83 <sup>b</sup> ; 374.37 <sup>c</sup> ; 374.94 <sup>a</sup> ; 375.05 <sup>e</sup>		342.75 (-8%)
$z_{\text{Fe}}$	0.22021(09) <sup>b</sup> ; 0.22046(8) <sup>d</sup> ; 0.22067(8) <sup>c</sup> ; 0.2209(5) <sup>e</sup> ; 0.2209(6) <sup>f</sup> ; 0.2212(15) <sup>a</sup> ;	0.25	0.227 (-20%)
$x_{\text{O}}$	0.443(2) <sup>a</sup> ; 0.44506(22) <sup>d</sup> ; 0.4453(8) <sup>f</sup> ; 0.44582(22) <sup>c</sup> ; 0.4460(8) <sup>e</sup> ; 0.44694(28) <sup>b</sup>	0.5	0.436 (+12%)
$y_{\text{O}}$	0.012(4) <sup>a</sup> ; 0.01700(28) <sup>c</sup> ; 0.0173(12) <sup>e</sup> ; 0.01789(28) <sup>d</sup> ; 0.01814(35) <sup>b</sup> ; 0.0185(13) <sup>f</sup>	0.0	0.018 (±0%)
$z_{\text{O}}$	0.9511(5) <sup>f</sup> ; 0.9513(5) <sup>e</sup> ; 0.95152(11) <sup>d</sup> ; 0.95183(14) <sup>b</sup> ; 0.95183(11) <sup>c</sup> ; 0.9543(20) <sup>a</sup>	0.0	0.961 (-15%)
$\alpha$ (°)	59.34 <sup>c</sup> ; 59.35 <sup>b</sup> ; 59.35 <sup>e</sup> ; 59.39 <sup>d</sup> ; 59.39 <sup>f</sup> ; 59.42 <sup>a</sup>	60	59.89 (-81%)
$\omega$ (°)	12.2 <sup>e</sup> ; 12.3 <sup>b</sup> ; 12.4 <sup>c</sup> ; 12.5 <sup>a</sup> ; 12.5 <sup>f</sup> ; 12.6 <sup>d</sup>	0	14.4 (+14%)
$P$	$\approx 100$ <sup>g</sup> ;		94

<sup>a</sup> Moreau *et al.* [1]. Single crystal X-Ray and neutron powder diffraction at room temperature.

<sup>b</sup> Palewicz *et al.* [2]. Neutron powder diffraction at 298 K.

<sup>c</sup> Palewicz *et al.* [3]. Neutron powder diffraction at 298 K.

<sup>d</sup> Palewicz *et al.* [3]. Neutron powder diffraction at 5 K.

<sup>e</sup> Fischer *et al.* [4]. Neutron powder diffraction at 293 K.

<sup>f</sup> Fischer *et al.* [4]. Neutron powder diffraction at 4.2 K.

<sup>g</sup> Lebeugle *et al.* [5]. Single crystals,  $R3c$  phase, room temperature.

TABLE I. Measured (ordered by size) and calculated structure parameters of BiFeO<sub>3</sub> in the  $R3c$  phase: Hexagonal lattice constants  $a$  and  $c$ ,  $c/a$  ratio, cell volume  $V$ , fractional atomic coordinates, rhombohedral cell angle  $\alpha$ , octahedral rotation angle  $\omega$ , and ferroelectric polarization  $P$ . Errors (in brackets) are with respect to the closest experimental value. Errors of atomic coordinates,  $\alpha$ , and  $c/a$  are those of ferroelectric distortions from the ideal perovskite structure.

### Electronic and lattice screening

The screening (the real part of the static dielectric constant  $\epsilon$ ) is calculated *ab initio* using the primitive rhombohedral cell and a  $k$ -point mesh of  $10 \times 10 \times 10$  points.  $\epsilon$  is diagonal in the coordinate system spanned by the hexagonal lattice vectors (the pseudocubic  $[111]$ ,  $[\bar{1}10]$ , and  $[\bar{1}\bar{1}2]$  directions, parallel and perpendicular to the ferroelectric polarization). The electronic contribution  $\epsilon^e$  has the eigenvalues 7.4, 8.1, and 8.1, the lattice (ionic) contribution has the eigenvalues 21, 37, and 37. In order to obtain the screening in the direction  $s$  perpendicular to a domain wall, one needs to rotate  $\epsilon$  and obtains

type	$n_{\text{atoms}}$	$E$ (mJ/m <sup>2</sup> )		$\xi_P$ (Å)	$\xi_A$ (Å)
		this work	Lit.		
71°	80	167	152 <sup>a</sup> , 156 <sup>d</sup>	2.94±0.01	3.4±0.7
71°	100	170		2.94±0.05	2.4±0.4
71°	120	172	167 <sup>a</sup> , 143.2 <sup>c</sup>	2.94±0.04	2.6±0.3
71°	160		128 <sup>b</sup>		
109°	80	60	62 <sup>a</sup> , 53 <sup>d</sup>	1.8±0.2	0.4
109°	100	60		2.0±0.1	0.4
109°	120	63	62 <sup>a</sup> , 52.9 <sup>c</sup>	1.9±0.1	0.1
109°	160		33 <sup>b</sup>		
180°	80	94	74 <sup>a</sup> , 71 <sup>d</sup>	1.63±0.06	–
180°	100	86		1.67±0.05	–
180°	120	84	82 <sup>a</sup> , 81.9 <sup>c</sup>	1.67±0.04	–
180°	140	86		1.67±0.04	–
180°	160		98 <sup>b</sup>		

<sup>a</sup> Diéguez *et al.* [7], LDA+ $U$ ,  $U=4$  eV

<sup>b</sup> Wang *et al.* [6], GGA+ $U$ ,  $U=7$  eV,  $J=1$  eV

<sup>c</sup> Chen *et al.* [8], GGA+ $U$ ,  $U=3$  eV

<sup>d</sup> Ren *et al.* [9], LDA+ $U$ ,  $U=3.87$  eV

TABLE II. DW energies  $E$  and DW widths ( $\xi_P$ : polarization,  $\xi_A$ : tilt wall width) as function of the supercell size. Errors are standard errors of the fit.

$n_{\text{atoms}}$	$-\Delta V_e^{\text{DW}}$ (mV)		$d_{\text{DW}}$ (Å)	
	71°	109°	71°	109°
160	187	-18.3	22.1	31.2
200	159	-5.8	27.6	39.0
240	150	2.9	33.2	46.8
280	157	5.6	38.7	54.6
$\infty$	133	17.3	$\infty$	$\infty$

TABLE III. Electrostatic open-circuit potential step  $-\Delta V_e^{\text{DW}}$  of the 71° and 109° domain walls without excitons as a function of the domain-wall distance  $d_{\text{DW}}$  (the number of atoms in the supercell,  $n_{\text{atoms}}$ ), as depicted in Fig. 3.

$\epsilon_{ss}^e = 7.6$ ,  $\epsilon_{ss}^{\text{ion}} = 26$ , and  $\epsilon_{ss}^{\text{total}} = 34$  for the 71° domain wall and  $\epsilon_{ss}^e = 7.9$ ,  $\epsilon_{ss}^{\text{ion}} = 32$ , and  $\epsilon_{ss}^{\text{total}} = 40$  for the 109° domain wall. Both in the case of the polarization-based potential in the ground state and in the case of the photovoltage, screening is included *a posteriori*. For the polarization-based potential we use  $\epsilon_{\text{total}}^{ss}$ , for the photovoltages we use an effective dielectric constant  $\epsilon_{ss}^{\text{eff}}$  that replaces the electronic screening  $\epsilon_{ss}^e$  that is automatically included by the total (electronic and lattice) screening:

$$\epsilon_{ss}^{\text{eff}} = \frac{\epsilon_{ss}^{\text{ion}} + \epsilon_{ss}^e}{\epsilon_{ss}^e}. \quad (5)$$

The effective dielectric constant is  $\epsilon_{ss}^{\text{eff}} = 4.4$  for the 71° DW and  $\epsilon_{ss}^{\text{eff}} = 5.0$  for the 109° DW.

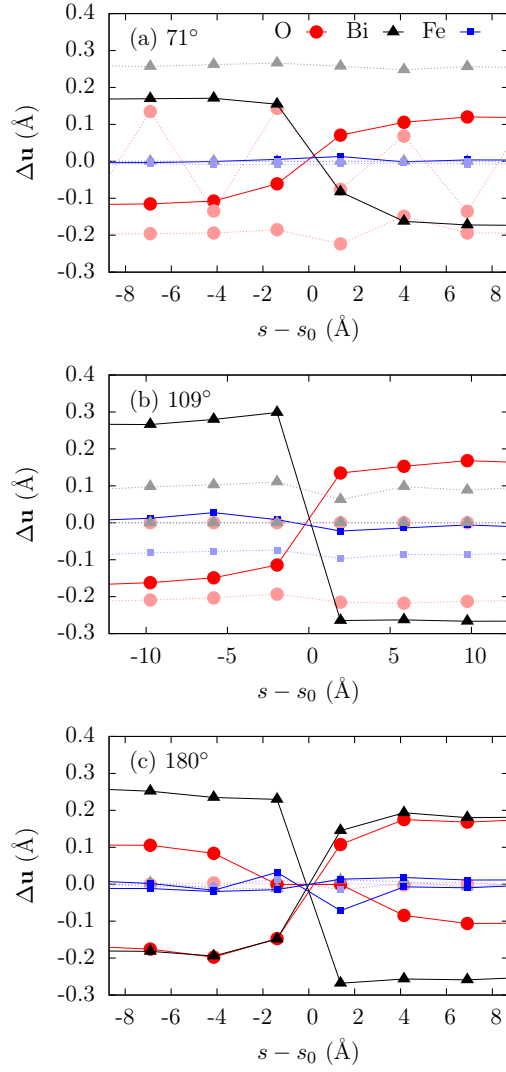


FIG. 1. The three cartesian components of the atomic displacements from the paraelectric, tilt-free phase in each atomic layer (a) for the  $71^\circ$  domain wall, (b) for the  $109^\circ$  domain wall, and (c) for the  $180^\circ$  domain wall in the coordinate system spanned by the supercell vectors: pseudocubic  $[110]$ ,  $[\bar{1}10]$ , and  $[001]$  directions ( $71^\circ$  wall);  $[100]$ ,  $[011]$ , and  $[0\bar{1}1]$  ( $109^\circ$  wall);  $[\bar{1}\bar{1}0]$ ,  $[110]$ , and  $[001]$  ( $180^\circ$  wall). Components that nominally remain constant across the domain wall are transparent.  $s_0$  is the position of the domain wall.

### Excitonic densities

Figure 4 shows the densities of excess electron and hole for an exciton at the  $109^\circ$  domain wall. Similar to the case of the  $71^\circ$  wall (see Fig. 3 in the main article), a small exciton polaron forms spontaneously.

### Photovoltage

Figures 5 and 6 show all calculated photovoltage profiles for the  $71^\circ$  and the  $109^\circ$  domain wall in the 280-atom super-

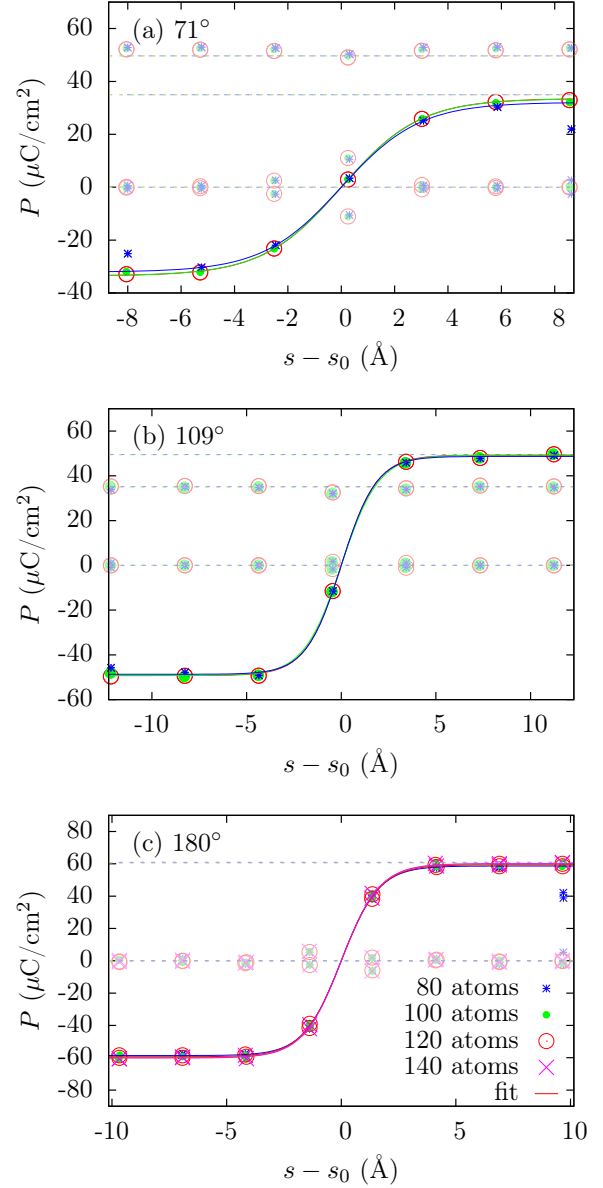


FIG. 2. Polarization  $P$  profiles for different supercell sizes (a) for the  $71^\circ$ , (b) for the  $109^\circ$  domain wall, and (c) for the  $180^\circ$  wall. Components that do not change sign at the domain wall are drawn transparent. Dashed transparent lines are the bulk reference. The profiles were fit according to Eq. (1).  $s_0$  is the position of the domain wall.

cell.

The open-circuit (OC) voltage profiles were obtained from the short-circuit (SC) voltage profiles by adding a constant gradient such that in the domain interior the resulting OC voltage slope vanishes, as depicted in Fig. 7.

Table IV contains the calculated short-circuit and open-circuit domain-wall photovoltages obtained with different supercell sizes (different domain-wall distances), and those extrapolated to the limit of infinitely large domain-wall distances. In the case of the  $71^\circ$  domain wall the extrapolated

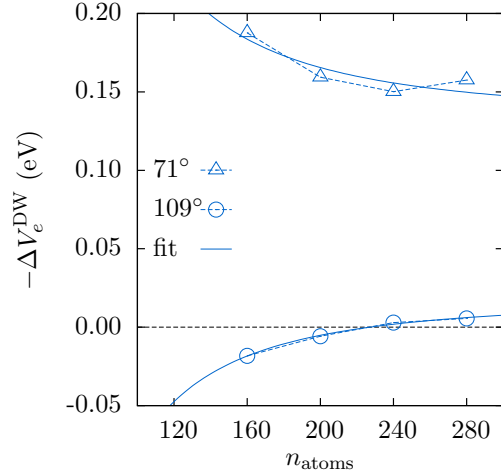


FIG. 3. Electrostatic potential step (electronic potential drop) at the 71° and the 109° domain wall without excitons as a function of the number of atoms  $n_{\text{atoms}}$  in the supercell (which is proportional to the domain-wall distance).

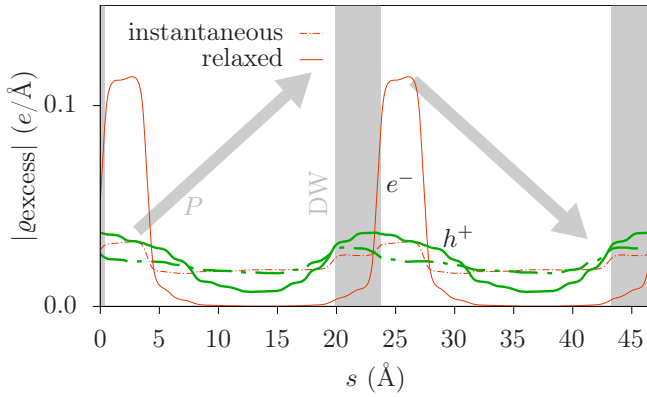


FIG. 4. Smoothened densities of excess electron and hole for excitons ( $X$ ) at the 109° domain wall before (“instantaneous”) and after (“relaxed”) polaron formation for an  $X$  density of 1  $X$  per 120-atom supercell ( $\approx 3.3 \cdot 10^{14}$   $X/\text{cm}^2$ ).

voltages (numbers in **boldface** in Tab. IV) are depicted in Fig. 7 in the main article. In the case of the 109° domain wall it is not possible to perform such an extrapolation because there is no strongly confining potential slope. Instead we depict the range of photovoltages between that of the largest supercell (280 atoms), and the largest photovoltage as a function of supercell size (numbers in **boldface** in Tab. IV).

#### Parameters used in the rate equation

*Light penetration depth in a BiFeO<sub>3</sub> film* The penetration depth calculated from our first-principles absorption coeffi-

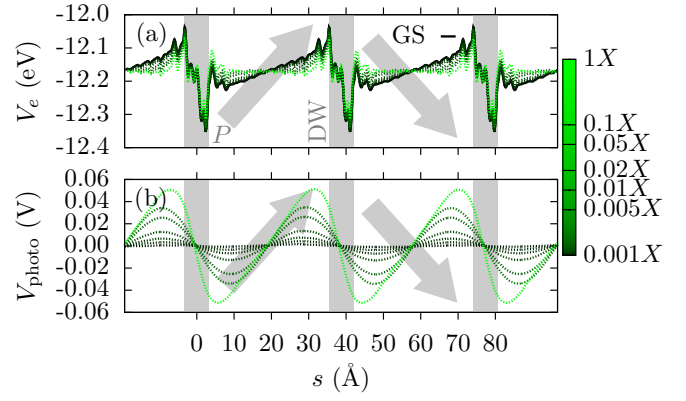


FIG. 5. (a) Ground-state and excited-state potential profile for exciton densities from 0.001 to 1 excitons ( $X$ ) per 280-atom supercell with 71° domain walls, (b) photovoltage profiles for these densities.

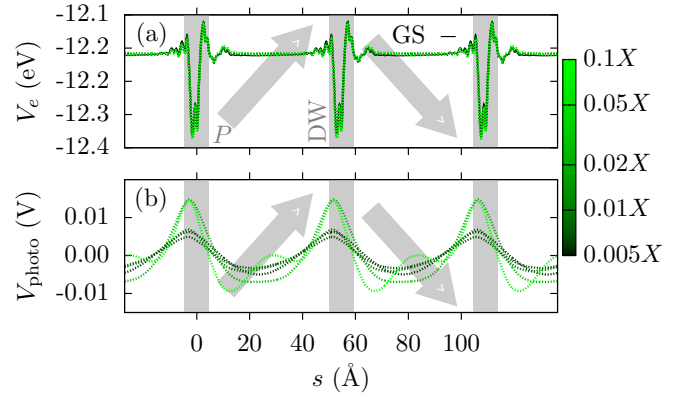


FIG. 6. The same as Fig. 5 for the 109° domain wall. Exciton densities range from 0.005  $X$  to 0.1  $X$  per supercell.

cient (which is similar to the one measured in Ref. 11) is about 33 nm at the photon energy of 3.06 eV that was used in experiment, such that about 95% of the penetrating light is absorbed in a 100 nm thick film. In Ref. 12 the penetration depth was estimated to be 50 nm, which would result in 86% of the penetrating light being absorbed.

*Carrier diffusion length* It is difficult to accurately estimate the photocarrier diffusion length  $l_{\text{diff}}$ , therefore two different numbers are considered in the main article. An upper boundary should be the length of a ferroelectric domain.

*Exciton density at the domain wall* The planar exciton density  $n_X^{\text{DW}}$  is given by the number of excitons  $N_X$  and the domain-wall area  $A_{\text{DW}}$  contained in the supercell,  $n_X^{\text{DW}} = N_X/(2A_{\text{DW}})$ . The domain-wall area is  $A_{\text{DW}} \approx 42.7 \text{ \AA}^2$  for the 71° domain wall and  $A_{\text{DW}} \approx 30.2 \text{ \AA}^2$  for the 109° domain wall. Assuming that all photocarriers within  $l_{\text{diff}}$  reach the domain walls, the exciton density can be expressed as  $n_X = n_X^{\text{DW}}/l_{\text{diff}}$ , where  $n_X^{\text{DW}}$  is the planar exciton density at the domain wall. Then Eq. (3) in the main article becomes

$$I_{\text{light}} = \frac{n_X^{\text{DW}} E_{\text{photon}} d_{\text{film}}}{l_{\text{diff}}(1-R)\tau}. \quad (6)$$

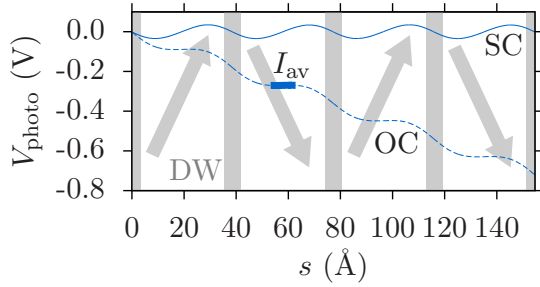


FIG. 7. Short-circuit (SC) photovoltage profile (thin solid line), open-circuit (OC) photovoltage profile (dashed line) for a 280-atom supercell with 71° domain walls, and the interval  $I_{av}$  (thick solid line) in which the average voltage slope was compensated by a constant gradient.

### Extrapolation of domain-wall photovoltages to large domain-wall distances

Figure 8 shows the open-circuit photovoltage as a function of the distance between two 71° domain walls  $d_{DW}$ . The photovoltage does not yet converge for our employed  $d_{DW}$  (supercells with up to 280 atoms), therefore we extrapolate it to the limit of large  $d_{DW}$  by means of a fit function:

$$V_{\text{photo}}^{\text{DW}}(d_{\text{DW}}) = V_{\text{photo}}^{\text{DW}}(\infty) - \Delta V_{\text{photo}}^{\text{DW}} e^{-b d_{\text{DW}}^{3/2}}, \quad (7)$$

where  $V_{\text{photo}}^{\text{DW}}(\infty)$ ,  $\Delta V_{\text{photo}}^{\text{DW}}$ , and  $b$  are fit parameters.  $V_{\text{photo}}^{\text{DW}}(\infty)$  is the extrapolated domain-wall photovoltage that is used in the main article. The fit function was chosen based on the exponential decay of the wave function of a particle in a linear potential (Airy function [13]). The data for the largest considered  $X$  density of 1  $X$  per supercell could not be extrapolated to large  $d_{DW}$  and were therefore left out of the analysis. In the case of the 109° domain wall, see Fig. 9, the domain-wall photovoltage increases, then decreases with increasing domain-wall distance. Here we cannot easily extrapolate to large domain-wall distances, instead we consider the maximum photovoltage as a function of supercell size as an upper limit. As a lower limit we take the photovoltage of the largest considered domain-wall distance.

### Extrapolation of domain-wall photovoltages to low light intensities

The photovoltages shown in Fig. 7 in the main article were extrapolated to low exciton densities (low light intensities  $I$ ) with a power law of the form

$$V_{\text{photo}}^{\text{DW}}(I) = V_{\text{photo}}^{\text{DW}}(I_0) \left( \frac{I}{I_0} \right)^p \quad (8)$$

$n_X$	$n_{\text{atoms}}$	71° DW				109° DW			
		SC <sub>us</sub>	OC <sub>us</sub>	OC	$d_{\text{DW}}$ (Å)	SC <sub>us</sub>	OC <sub>us</sub>	OC	$d_{\text{DW}}$ (Å)
0.005	120	1.47	3.68	0.829	16.6	2.47	-0.281	-0.0558	23.4
	160				22.1				31.2
	200	3.86	11.0	2.48	27.6	5.77	12.4	2.46	39.0
	240	5.76	15.1	3.40	33.2	6.47	15.7	<b>3.12</b>	46.8
	280	7.85	18.1	4.08	38.7	11.7	5.36	<b>1.06</b>	54.6
	∞		23.9	<b>5.38</b>	∞				∞
0.01	120	2.90	7.28	1.64	16.6	4.85	0.03	0.00596	23.4
	160	4.03	10.3	2.32	22.1				31.2
	200	7.16	20.4	4.60	27.6	10.9	21.0	4.17	39.0
	240	10.8	29.1	6.56	33.2	14.2	26.0	<b>5.17</b>	46.8
	280	14.4	36.0	8.11	38.7	8.49	6.13	<b>1.22</b>	54.6
	∞		52.9	<b>11.9</b>	∞				∞
0.02	120	5.66	14.2	3.20	16.6	8.92	-0.39	-0.0775	23.4
	160				22.1				31.2
	200	13.3	37.5	8.45	27.6	17.6	35.4	<b>7.03</b>	39.0
	240	20.1	54.7	12.3	33.2	20.2	33.3	6.62	46.8
	280	26.5	68.9	15.5	38.7	11.4	8.69	<b>1.73</b>	54.6
	∞		111	<b>25.0</b>	∞				∞
0.05	120	13.2	33.2	7.48	16.6	17.1	1.58	0.314	23.4
	160				22.1				31.2
	200	28.2	79.1	17.8	27.6	28.7	50.9	10.1	39.0
	240	41.1	113	25.5	33.2	33.6	53.8	<b>10.7</b>	46.8
	280	52.0	138	31.1	38.7	22.7	3.95	<b>0.785</b>	54.6
	∞		186	<b>41.9</b>	∞				∞
0.1	120	23.8	59.7	13.5	16.6	26.3	-3.04	0.604	23.4
	160	28.5	77.0	17.3	22.1	21.8	20.7	4.11	31.2
	200	44.2	123	27.7	27.6	38.0	54.9	<b>10.9</b>	39.0
	240	59.4	162	36.5	33.2	38.2	35.4	7.03	46.8
	280	69.3	180	40.6	38.7	24.2	23.4	<b>4.65</b>	54.6
	∞		193	<b>43.5</b>	∞				∞
1	120	83.8	165	37.2	16.6				23.4
	160	83.8	173	39.0	22.1				31.2
	200	90.9	175	39.4	27.6				39.0
	240	98.1	189	42.6	33.2				46.8
	280	102	172	38.8	38.7				54.6

TABLE IV. Calculated short-circuit (SC) and open-circuit (OC) domain-wall photovoltages  $V_{\text{photo}}^{\text{DW}}$  for different domain-wall distances  $d_{\text{DW}}$  (different numbers of atoms  $n_{\text{atoms}}$  in the supercell) and extrapolations to infinitely large domain-wall distances as a function of the number of excitons  $n_X$  per supercell for the 71° and the 109° domain walls. Unscreened voltages are marked by the subscript “us”, such as SC<sub>us</sub>. The photovoltages printed in **boldface** are the ones drawn in Fig. 7 in the main article.

that was optimized using the three data points corresponding to the lowest light intensities. In the case of the 71° domain wall  $p \approx 1.14$ . The photovoltage data of the 109° DW exhibit too much noise to safely extrapolate them to low light intensities.

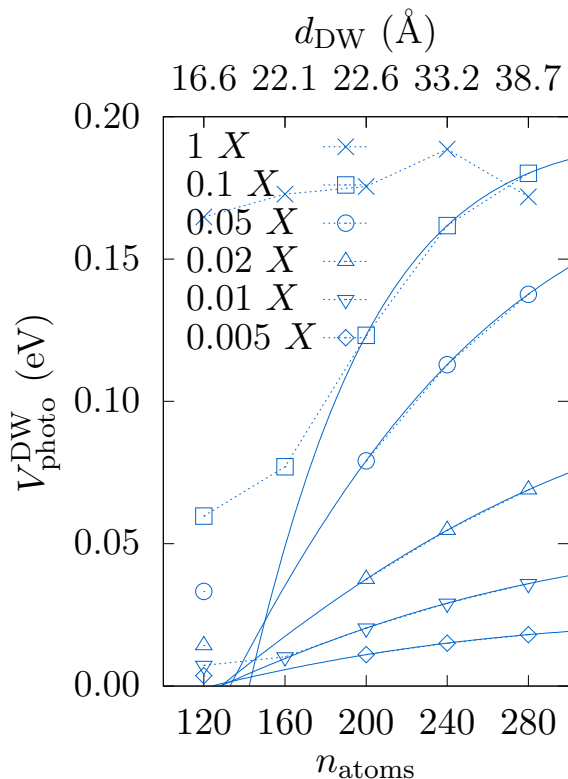


FIG. 8. Open-circuit photovoltage of the  $71^\circ$  domain wall as a function of the number of atoms  $n_{\text{atoms}}$  in the supercell and of the distance between domain walls,  $d_{\text{DW}}$  (data points from Table IV). Solid lines are fits with Eq. (7), dotted lines are a guide to the eye.

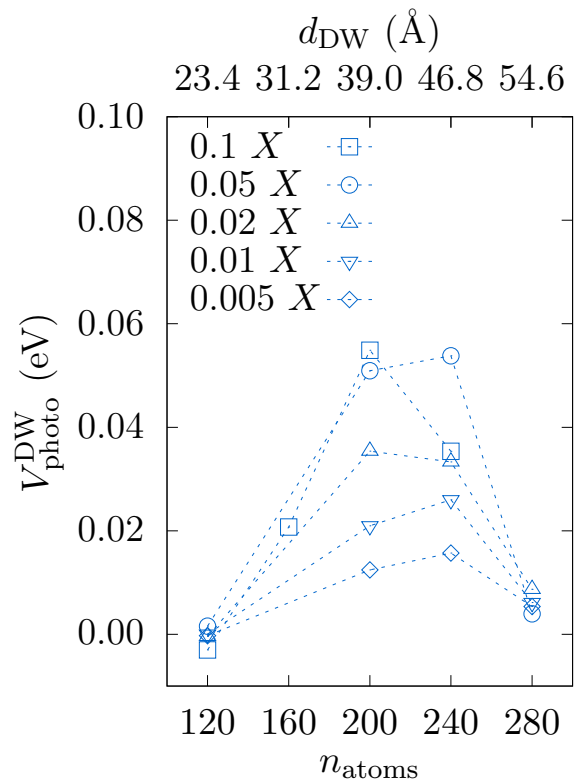


FIG. 9. The same as Fig. 8 for the  $109^\circ$  domain wall. Note the change of scale.

### Smoothing of charge densities and potential

The rapid and strong oscillations of charge densities and electronic potential at atomic nuclei, which obscure variations on a larger scale, were smoothed in the following way: First the charge density or potential was averaged in a plane parallel to the domain-wall plane [in the  $r$ - $t$  plane, compare Figs. 1(a) and 2(a) in the main article], then a sliding-window average over an  $s$  interval of one atomic plane spacing, like in Ref. [10], was applied to the excess charge carrier densities. In order to smoothen the potential a low-pass filter was applied that removed wavelengths up to one atomic plane spacing. The two smoothening methods should be roughly equivalent, and it is only for historical reasons that one was used for the densities and the other for the potential.

### Self-trapping at low carrier concentrations

Charge carriers become spontaneously self-trapped for all carrier concentrations considered. Figure 10 shows the iso-surface of the charge density of an excess electron in a 320-atom supercell, the lowest carrier concentration considered.

\* skoerbel@uni-muenster.de

- [1] J. M. Moreau, C. Michel, R. Gerson, and W. J. James, "Ferroelectric  $\text{BiFeO}_3$  X-ray and neutron diffraction study," *Journal of Physics and Chemistry of Solids* **32**, 1315 – 1320 (1971).
- [2] Andrzej Palewicz, R. Przeniosło, Izabela Sosnowska, and AW Hewat, "Atomic displacements in  $\text{BiFeO}_3$  as a function of temperature: neutron diffraction study," *Acta Crystallographica Section B: Structural Science* **63**, 537–544 (2007).
- [3] A. Palewicz, I. Sosnowska, R. Przeniosło, and AW Hewat, " $\text{BiFeO}_3$  crystal structure at low temperatures," *Acta Physica Polonica-Series A General Physics* **117**, 296 (2010).
- [4] P. Fischer, M. Polomska, I. Sosnowska, and M. Szymanski, "Temperature dependence of the crystal and magnetic structures of  $\text{BiFeO}_3$ ," *Journal of Physics C: Solid State Physics* **13**, 1931 (1980).
- [5] Delphine Lebeugle, Dorothée Colson, A. Forget, and Michel Viret, "Very large spontaneous electric polarization in  $\text{BiFeO}_3$  single crystals at room temperature and its evolution under cycling fields," *Appl. Phys. Lett.* **91**, 022907 (2007).
- [6] Yi Wang, Chris Nelson, Alexander Melville, Benjamin Winchester, Shunli Shang, Zi-Kui Liu, Darrell G. Schlom, Xiaoqing Pan, and Long-Qing Chen, " $\text{BiFeO}_3$  domain wall energies and structures: a combined experimental and density functional theory+U study," *Phys. Rev. Lett.* **110**, 267601 (2013).
- [7] Oswaldo Diéguez, Pablo Aguado-Puente, Javier Junquera, and Jorge Íñiguez, "Domain walls in a perovskite oxide with two primary structural order parameters: First-principles study of

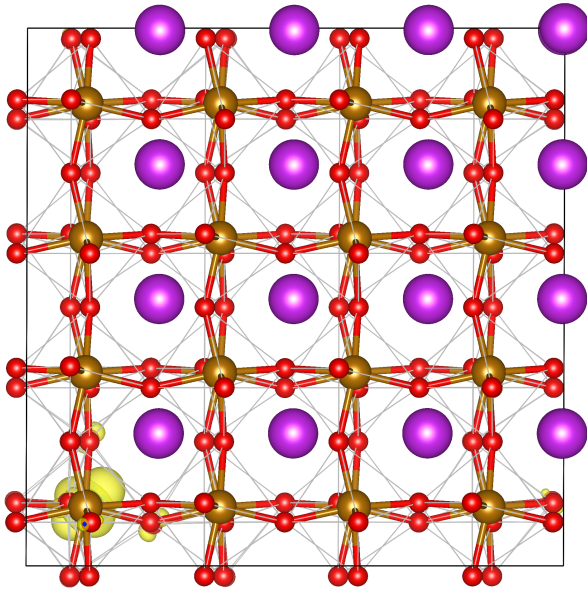


FIG. 10. Self-trapped electron in a 320-atom supercell (yellow: charge density iso-surface of the excess electron, large purple spheres: Bi, medium-sized brown spheres: Fe, small red spheres: O).

- BiFeO<sub>3</sub>,” *Phys. Rev. B* **87**, 024102 (2013).
- [8] Yun-Wen Chen, Jer-Lai Kuo, and Khian-Hooi Chew, “Polar ordering and structural distortion in electronic domain-wall properties of BiFeO<sub>3</sub>,” *J. Appl. Phys.* **122**, 075103 (2017).
- [9] Wei Ren, Yurong Yang, Oswaldo Diéguez, Jorge Íñiguez, Narayani Choudhury, and L. Bellaiche, “Ferroelectric Domains in Multiferroic BiFeO<sub>3</sub> Films under Epitaxial Strains,” *Phys. Rev. Lett.* **110**, 187601 (2013).
- [10] B Meyer and David Vanderbilt, “Ab initio study of ferroelectric domain walls in PbTiO<sub>3</sub>,” *Phys. Rev. B* **65**, 104111 (2002).
- [11] V Železný, D Chvostová, L Pajasová, I Vrejoiu, and M Alexe, “Optical properties of epitaxial BiFeO<sub>3</sub> thin films,” *Applied Physics A* **100**, 1217–1220 (2010).
- [12] Marin Alexe and Dietrich Hesse, “Tip-enhanced photovoltaic effects in bismuth ferrite,” *Nature Communications* **2**, 256 (2011).
- [13] Wolfgang P. Schleich, *Quantum Optics in Phase Space, Appendix E* (WILEY-VCH Verlag Berlin GmbH, 2001).